JACS
JOURNAL OF THE AMERICAN CHEMICAL SOCIETY
Article
Cite This: J. Am. Chem. Soc. 2018, 140, 2206−2213
pubs.acs.org/JACS

Organic Mixed Valence Compounds Derived from Cyclic (Alkyl)(amino)carbenes

Max M. Hansmann, Mohand Melaimi, and Guy Bertrand*

UCSD-CNRS Joint Research Laboratory (UMI 3555), Department of Chemistry and Biochemistry, University of California, San Diego, La Jolla, California 92093-0358, United States

Supporting Information

ABSTRACT: Readily available room temperature stable organic mixed valence compounds are prepared by one-electron reduction of cyclic bis(iminium) salts [derived from cyclic (alkyl)(amino)carbenes] bridged by various spacers. These compounds show characteristic intervalence charge transfer (IV-CT) bands in the near-infrared (NIR). Cyclic voltammetry, EPR, IR, UV−vis, and X-ray studies, as well as DFT calculations, show that, depending on the nature of the spacer, these mixed valence compounds range from class III to class II.

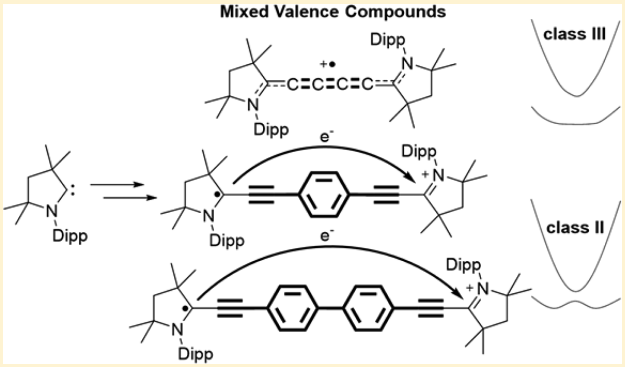

INTRODUCTION

Electron transfer is one of the most fundamental processes in chemistry and has applications in various fields ranging from biology to electronic devices.[1] Mixed valence (MV) compounds **I** are ideal systems to systematically study the fundamental principles of electron transfer (Figure 1).[2] They contain a spacer between two or more identical redox active sites, and feature an open-shell ground state.[3] Since the pioneering work of Creutz and Taube,[4] MV systems have mostly been associated with discrete redox states at transition metal sites, as illustrated by complex **II**, whereas organic mixed valence compounds are less represented, presumably as a result of the instability of open-shell organic molecules.[5,6] Wurster's radical cation **III**,[7] tetrathiafulvalene radical cation **IV**,[8] or the *para*-quinone radical anion **V** are prominent representatives for delocalized organic radicals.[9] However, they might be better referred to as "charge-resonance" rather than MV compounds, since the radical is delocalized over the entire molecule and the redox sites are not clearly defined.[3] The nature of electron "localization" vs "delocalization" is fundamental to MV compounds and has led to the Robin−Day classification[10] in which any MV compound can be classified into one of three classes. Class I compounds exhibit two well separated redox sites in which the two centers cannot interact or the interaction is too small to be measured; class II compounds exhibit weakly interacting redox centers in which the charge is localized on one redox site; in class III compounds, both sites are so strongly coupled that the radical is fully delocalized over the entire molecule, leading to undistinguishable redox sites with intermediate redox states. On the basis of this classification, compounds **III**−**V** could be seen as class III MV systems. Importantly, while organic delocalized radical ions have been investigated by EPR spectroscopy since the 1950s, the concept of organic mixed valency was first clearly introduced in the 1990s with the spectroscopic analysis of intervalence charge transfer (IV-CT) bands as a result of

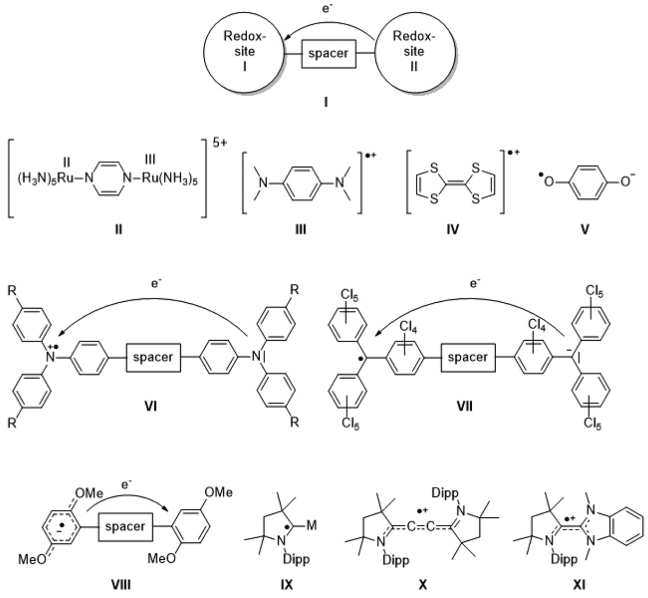

Figure 1. Schematic representation of MV compounds (**I**), Creutz−Taube MV complex (**II**), "charge-resonance" derivatives (**III**−**V**), organic mixed valence compounds (**VI**−**VIII**), and CAAC derived radicals (**IX**−**XI**).

Received: October 26, 2017
Published: January 17, 2018

DOI: 10.1021/jacs.7b11184
J. Am. Chem. Soc. 2018, 140, 2206−2213

Marcus–Hush theory.[11] The framework of this theory[12] provides the basis for the Robin–Day classification and allows one to predict and classify the class of mixed valency based on the shape of the IV-CT bands typically observed in the near-infrared (NIR) region. In general, organic MV compounds feature distinct IV-CT bands, while transition metal based MV compounds are typically more difficult to interpret, since overlapping transitions can occur.

In contrast to inorganic MV compounds, the open-shell character of organic MV compounds limits the chemical space to only a few molecules with stable organic radical redox sites. Among them, due to their stability and easy synthetic access, radical cations of tertiary triaryl-amines (**VI**) have been exploited, for example, as photoconductors and light-emitting devices.[13] As it is difficult to stabilize carbon centered radicals, such organic MV compounds are significantly less studied; however, some notable examples are perchlorinated triphenyl-methyl **VII**[14] and 1,4-dimethoxybenzene derived radicals **VIII**.[15] Our group and others have demonstrated that cyclic (alkyl)(amino)carbenes (CAACs)[16,17] are excellent ligands for stabilizing a variety of organic,[18] main-group and transition metal paramagnetic species (**IX**).[19,20] In 2014, Roesky et al. and our group independently reported the synthesis of the fully delocalized air stable radical cation **X**.[21] Together with radical cation **XI**,[22] these compounds could be considered as charge-resonance compounds based upon CAACs. In contrast, herein we report the synthesis and first spectroscopic characterization of a novel family of organic compounds derived from CAACs, which fulfill the spectroscopic requirements for MV compounds.

RESULTS AND DISCUSSION

Recently, we described a modular approach for the synthesis of bis(alkynyl)(iminium) salts **4** based on the "click"-type coupling of terminal diynes **2** with CAACs **1**, followed by hydride abstraction (Scheme 1).[23] We reported that two-electron reduction afforded derivatives **5**, whose ground state can be described as a singlet-closed/open shell compound.

Scheme 1. Previously Reported Modular Approach toward Bis(iminium) Salts 4 and the Ensuing Diradicaloids 5

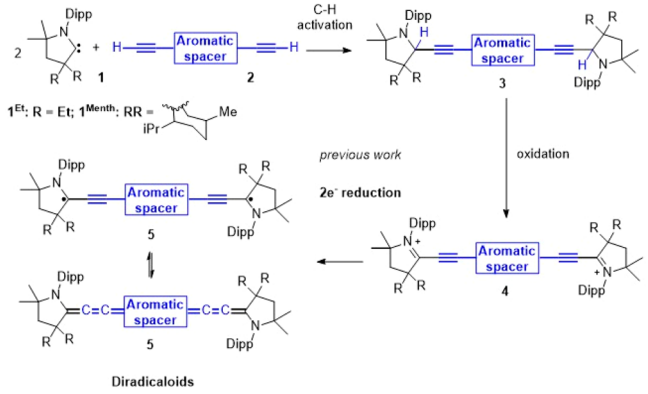

While the two-electron reduction of $\mathbf{4a}^{\mathbf{Et}}$ and $\mathbf{4a}^{\mathbf{Menth}}$ gave rise to $\mathbf{5a}^{\mathbf{Et}}$ and $\mathbf{5a}^{\mathbf{Menth}}$, respectively, we noted that the cyclic voltammogram of $\mathbf{4a}^{\mathbf{Et}}$ and $\mathbf{4a}^{\mathbf{Menth}}$ showed a relatively large separation of the first and second reduction potentials [$E_{1/2}$ = −0.72, −0.98 V (versus Fc^+/Fc)]. This observation motivated us to study the one-electron reduction in the hope of accessing organic mixed valence species. Either addition of 1 equivalent of cobaltocene to a solution of $\mathbf{4a}^{\mathbf{Et}}$ or $\mathbf{4a}^{\mathbf{Menth}}$ or stirring these compounds with freshly activated zinc dust gave rise to red colored solutions of $\mathbf{6a}^{\mathbf{Et}}$ and $\mathbf{6a}^{\mathbf{Menth}}$ (Scheme 2).

Scheme 2. One-Electron Reduction of 4a Giving Mixed Valence Compounds 6a

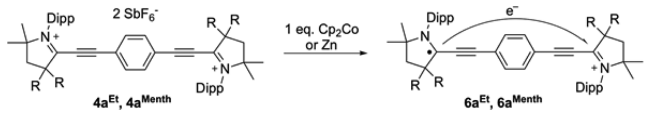

The UV–vis/NIR spectra of the three different oxidation states feature distinct differences (Figure 2). While dication $\mathbf{4a}^{\mathbf{Et}}$

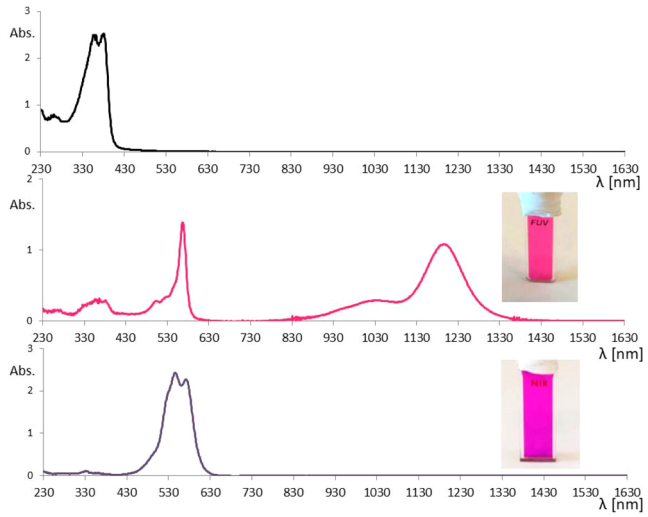

Figure 2. UV–vis/NIR absorption of dication $\mathbf{4a}^{\mathbf{Et}}$ in THF (top), radical-cation $\mathbf{6a}^{\mathbf{Et}}$ in THF (middle), and diradicaloid $\mathbf{5a}^{\mathbf{Et}}$ in pentane (bottom).

shows only an absorption band around 380 nm and $\mathbf{5a}^{\mathbf{Et}}$ has two intense absorption maxima at λ = 550 nm (log ε = 4.40 M^{-1} cm^{-1}), the radical cation $\mathbf{6a}^{\mathbf{Et}}$ shows an intense absorption maximum in the vis region at λ = 567 nm (log ε = 4.7 M^{-1} cm^{-1}) together with two broad Gaussian shaped NIR absorption bands at λ = 1020 and 1195 nm (log ε = 4.6 M^{-1} cm^{-1}). Such IV-CT absorption bands are characteristic for MV compounds.

Single crystals of $\mathbf{6a}^{\mathbf{Menth}}$ were obtained from a THF solution at −40 °C, and subjected to an X-ray diffraction study (Figure 3). Note that, compared to their inorganic counterparts, not many X-ray structural data are available for organic mixed valence systems. Interestingly, the solid state structure of $\mathbf{6a}^{\mathbf{Menth}}$ shows only moderate bond distance alterations when comparing the left and right parts of the molecule, while the average bond distances are positioned in between the bond distances reported[23] for dication $\mathbf{4a}^{\mathbf{Et}}$ and the neutral compound $\mathbf{5a}^{\mathbf{Menth}}$ (Figure 4).

Solutions of MV compounds $\mathbf{6a}^{\mathbf{Et}}$ and $\mathbf{6a}^{\mathbf{Menth}}$ are NMR silent and EPR active. The EPR spectra of the two radical cations $\mathbf{6a}^{\mathbf{Et}}$ and $\mathbf{6a}^{\mathbf{Menth}}$ appeared to be quite different due to an additional coupling to one of the H atoms of the menthyl group (C_2), as already observed[23,24] for diradicaloid $\mathbf{5a}^{\mathbf{Menth}}$ (Figure 5). Simulation[25] of the EPR spectrum (fit with >99% agreement) allowed for the extraction of the isotropic hyperfine

DOI: 10.1021/jacs.7b11184
J. Am. Chem. Soc. 2018, 140, 2206–2213

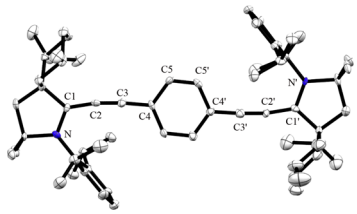

Figure 3. Solid-state structure of **6a**$^{\text{Menth}}$. Solvent molecules (THF), hydrogen atoms, and the counteranion (SbF_6^-) are omitted for clarity. Selected bond distances (Å) and angles (deg): N−C1 1.329(7), N′−C1′ 1.343(7), C1−C2 1.385(6), C1′−C2′ 1.372(7), C2−C3 1.220(7), C2′−C3′ 1.226(7), C3−C4 1.395(7), C3′−C4′ 1.405(7), C4−C5 1.405(7), C4′−C5′1.408(7), C5−C5′ 1.390(6), N−C1−C2 119.4(5), C1−C2−C3 169.8(6), C2−C3−C4 174.5(6).

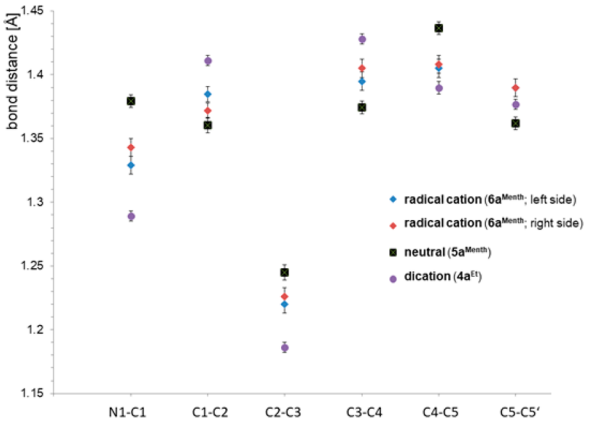

Figure 4. Comparison of bond distances for **4a**$^{\text{Et}}$, **5a**$^{\text{Menth}}$, and **6a**$^{\text{Menth}}$.

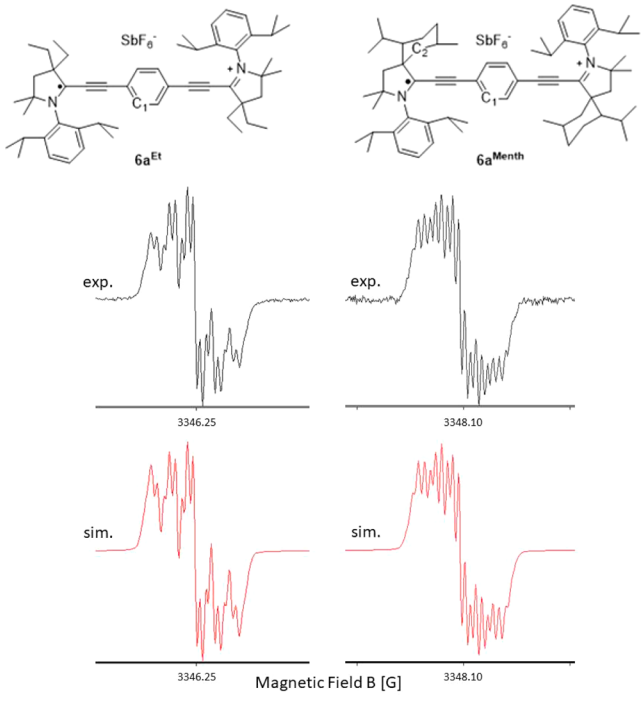

Figure 5. X-band EPR spectra (room temperature in THF) of radical cations **6a**$^{\text{Et}}$ and **6a**$^{\text{Menth}}$ (top) and their simulation (bottom).

coupling constants with a C_2 symmetrical environment [**6a**$^{\text{Et}}$: 2 N (a_N = 2.70G) and 4 H (a_H = 0.94G); **6a**$^{\text{Menth}}$: 2 N (a_N = 2.78G), 4 H (a_H = 0.92G), and 2 H (a_H = 1.16G)]. Importantly, these hyperfine coupling constants are in good agreement with the DFT calculated parameters at the B3LYP/TZVP level of theory (see the Supporting Information).

It should be noted that the hyperfine coupling constants with nitrogen (a_N ∼ 2.75 G) are significantly smaller than those observed in CAAC derived radical species (a_N ∼ 5.4−6.4 G).[18] The hyperfine coupling constants being derived from a symmetrical structure and the low amount of spin density on nitrogen clearly demonstrate the delocalization of the radical center through the entire system at the EPR time scale. This is also in agreement with the calculated SOMO at the UB3LYP/def2-TZVP level of theory (Figure 6). Spin densities calculated

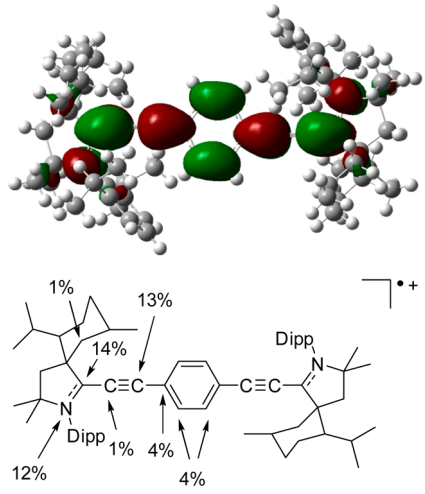

Figure 6. SOMO of **6a**$^{\text{Menth}}$ at the UB3LYP/def2-TZVP level of theory (isovalues 0.02) based on the structure determination by X-ray diffraction (top) and calculated Mulliken spin densities (bottom).

by Mulliken population analysis predict a well equilibrated spin density distribution with approximately 50% on the central CC−Ph−CC spacer and the remaining 50% spin density on the two CAAC moieties (Figure 6).

Since X-ray crystallography, EPR spectroscopy, and DFT calculations indicate a symmetrical structure in which the CAAC redox centers are strongly coupled, **6a**$^{\text{Et}}$ and **6a**$^{\text{Menth}}$ feature the attributes of class III MV compounds. However, EPR spectroscopy is a rather slow technique (10^{-9} s) for resolving the electron transfer processes, and X-ray analysis might give a superimposition of the two unsymmetrical radical cation structures. Additionally, standard functionals often overestimate delocalization as a result of the self-interaction error; they predict delocalized structures even in the case of class II MV compounds.[26] The most reliable classification is based on the analysis of the intervalence charge transfer (IV-CT) band in the NIR (Figures 2 and 7).

The IV-CT band of **6a**$^{\text{Menth}}$ in THF (λ_{max} = 1210 nm, $\tilde{\nu}_{max}$ = 8264 cm^{-1}) shows a perfect Gaussian shape without cutoff at the low energy side. Thus, a simple band shape analysis indicates that **6a**$^{\text{Menth}}$ is a class II MV system (note also that no vibrational fine structure was observed, which frequently occurs with class III systems). Furthermore, the observed solvent dependency ($\Delta\tilde{\nu}$(THF/dioxane) ca. 200 cm^{-1} [0.6 kcal/mol]) is in agreement with a dipole-moment change upon electron transfer, as expected for a class II MV system (Figure 7). According to Markus−Hush theory, it is possible to deduce the electronic coupling integral V from the IV-CT band on the basis of the absorption maximum $\tilde{\nu}_{max}$ (cm^{-1}), the bandwidth at

DOI: 10.1021/jacs.7b11184
J. Am. Chem. Soc. 2018, 140, 2206−2213

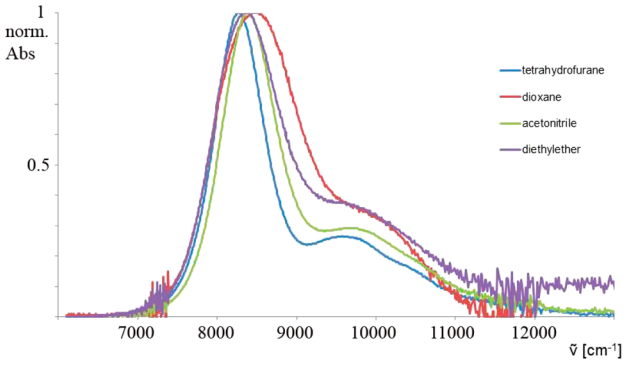

Figure 7. Solvent dependence of the IV-CT band of $\mathbf{6a}^{\mathbf{Menth}}$.

half-height $\tilde{\nu}_{1/2}$ (780 cm^{-1}), the molar absorptivity ε (43 427 M^{-1} cm^{-1}), and the distance r (10.7 Å; taken from the X-ray determination)[27] between the CAAC redox active centers according to formula I.[28]

$$V = \frac{0.0206}{r}\sqrt{\tilde{\nu}_{max}\tilde{\nu}_{1/2}\varepsilon} \quad \text{(I)}$$

Applying formula I for $\mathbf{6a}^{\mathbf{Menth}}$ leads to a coupling integral of V = 1019 cm^{-1} (for $\mathbf{6a}^{\mathbf{Et}}$, a similar value of V = 1032 cm^{-1} is obtained). This coupling integral fulfills with $2V/\lambda$ = 0.24 the requirement $0 < 2V/\lambda < (1 - \Delta\tilde{\nu}/\lambda)$ for a class IIa MV compound,[12] and shows a significant communication between the two CAAC redox active sites. It should be noted that the weaker high energy absorption band at $\lambda_{max} \sim 1043$ nm ($\tilde{\nu}_{max}$ = 9588 cm^{-1}) can be assigned to the electron transfer process from the CAAC radical center to the bridge based on analogy with other mixed valence systems[5] and a three-state model[12] seems reasonable to analyze the full system. As the herein studied compounds feauture alkyne moieties which show up in a characteristic region of the IR spectrum, this spectroscopy is a useful tool to evaluate the rate of electron transfer between the redox centers.[29] When the electron transfer is faster than the spectroscopic time scale (10^{-13} s), an averaging of the specific vibrational modes is observed. Upon reduction, the alkyne stretching band shifts from $\tilde{\nu}_{CC}$ = 2200 cm^{-1} ($\mathbf{4a}^{\mathbf{Et}}$) to a lower energy $\tilde{\nu}_{CC}$ = 2173 cm^{-1} ($\mathbf{6a}^{\mathbf{Et}}$), while full reduction to the neutral diradicaloid $\mathbf{5a}^{\mathbf{Et}}$ gives $\tilde{\nu}_{CC}$ = 2062 cm^{-1}. This shift is in agreement with a partial lowering of the bond order. We do not observe by ATR-IR for **5a** at room temperature two well-resolved IR absorptions for two different alkyne moieties, as expected for a slow electron transfer in a class II system (see the Supporting Information); however, in the case of $\mathbf{6a}^{\mathbf{Menth}}$, we observed a very broad IR band at $\tilde{\nu}_{CC}$ = 2079 cm^{-1}. These observations indicate that the intramolecular electron transfer rate at room temperature is at a similar rate or faster than ATR-IR spectroscopy. Furthermore, as this measurement was performed in the solid state and not in solution, the electron transfer process might be enhanced compared to solvent reorganization barriers.[29] Note MV systems based on transition metals and such a dialkynyl-benzene spacer also did not allow for a clear classification based on IR.[30]

In order to investigate the effect of the spacer on the communication between the CAAC redox sites, we investigated the one-electron reduction of $\mathbf{4b}^{\mathbf{Menth}}$, $\mathbf{4c}^{\mathbf{Menth}}$, and $\mathbf{4d}^{\mathbf{Et}}$, featuring spacers with different degrees of aromaticity and lengths, and we compared their properties with $\mathbf{4a}^{\mathbf{Menth}}$ (Figure 8). Note that $\mathbf{4d}^{\mathbf{Et}}$ which contains a 1,2-bisalkyne spacer has been prepared using the Glaser coupling (Scheme 3).

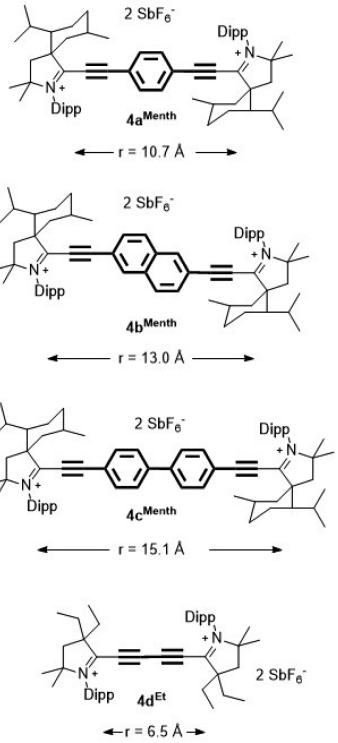

Figure 8. Spacers investigated and distances between the CAAC redox sites.

Scheme 3. Synthesis of Bis(iminium) Salt $\mathbf{4d}^{\mathbf{Et}}$

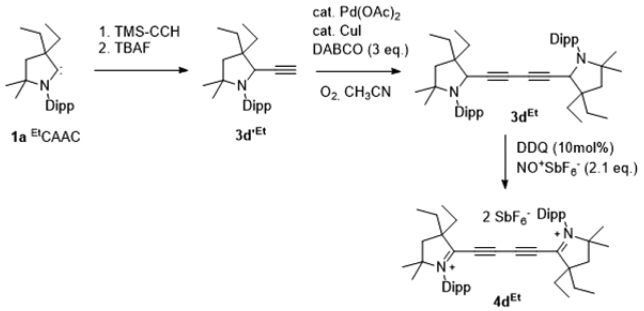

The cyclic voltammograms of **4a–d** show some distinct differences (Figure 9). As expected, increasing the length of the spacer from phenyl to naphthyl and biphenyl makes the first reduction significantly more difficult, while the second reduction potential remains nearly constant [$E_{1/2}$ = −0.68 V/−0.98 V ($\mathbf{4a}^{\mathbf{Menth}}$); −0.82 V/−1.03 V ($\mathbf{4b}^{\mathbf{Menth}}$); −0.99 V/−1.08 V ($\mathbf{4c}^{\mathbf{Menth}}$)]. In the case of the shorter spacer ($\mathbf{4d}^{\mathbf{Et}}$), the two reductions already proceed at −0.14 and −0.76 V with a large separation of ΔE = 620 mV.

On the basis of the CV, bis(iminium) salts $\mathbf{4b}^{\mathbf{Menth}}$, $\mathbf{4c}^{\mathbf{Menth}}$, and $\mathbf{4d}^{\mathbf{Et}}$ were reduced, using 1 equiv of cobaltocene, into the corresponding radical cations $\mathbf{6b}^{\mathbf{Menth}}$, $\mathbf{6c}^{\mathbf{Menth}}$, and $\mathbf{6d}^{\mathbf{Et}}$. Even though the two reduction potentials of $\mathbf{4c}^{\mathbf{Menth}}$ indicated a potential bistability (the differential pulse cyclovoltammogram shows two peaks; Figure S18), the reduction with 1 equiv of cobaltocene led to the desired radical cation $\mathbf{6c}^{\mathbf{Menth}}$. Note that cyclic voltammograms are typically not good indicators for mixed valence systems, as splittings might be dominated by electrostatic effects.[31]

All three compounds $\mathbf{6d}^{\mathbf{Et}}$, $\mathbf{6b}^{\mathbf{Menth}}$, and $\mathbf{6c}^{\mathbf{Menth}}$ are NMR silent but EPR active (Figure 10). The X-band EPR spectrum

DOI: 10.1021/jacs.7b11184
J. Am. Chem. Soc. 2018, 140, 2206–2213

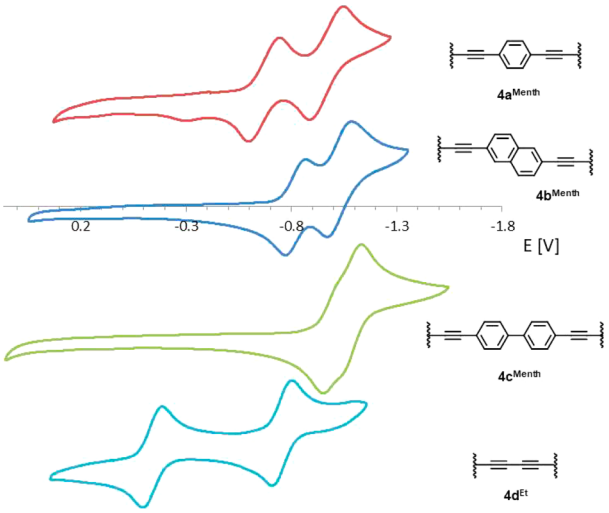

Figure 9. Cyclic voltammograms of bis-iminium salts **4a**^{Menth}, **4b**^{Menth}, **4c**^{Menth}, and **4d**^{Et} containing different spacer units (nBu$_4$NPF$_6$ 0.1 M in THF, 100 mV s^{-1}, vs Fc$^+$/Fc).

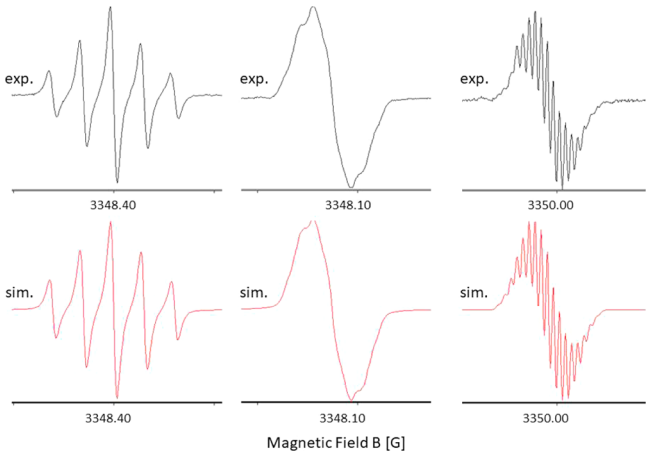

Figure 10. Experimental and simulated X-band EPR spectra of the MV compounds **6d**^{Et} (left), **6b**^{Menth} (middle), and **6c**^{Menth} (right) at room temperature in THF. **6d**^{Et}: 2 N (a_N = 4.14 G). **6b**^{Menth}: 2 N (a_N = 2.30 G), 2 H (a_H = 1.75 G), and 2 H (a_H = 1.0 G). **6c**^{Menth}: 2 N (a_N = 2.22 G), 4 H (a_H = 1.08 G), 4 H (a_H = 0.21 G), and 2 H (a_H = 2.24 G).

of **6d**^{Et} at room temperature in THF can be simulated with only two equal N (a_N = 4.14 G). Interestingly, the reported EPR spectrum of $[(^{Et}CAAC)_2C_2]^{+\bullet}$ exhibits the same hyperfine splitting pattern but with larger N-coupling constants (a_N = 5.3 G).[21] This is an indication of a decreased spin density on the nitrogen of **6d**^{Et} and thus a larger electron delocalization (Figure 11). Similarly, the nitrogen coupling constants decrease along the series **6a**^{Menth} (a_N = 2.70G), **6b**^{Menth} (a_N = 2.30 G), and **6c**^{Menth} (a_N = 2.22 G). The observed spin delocalization across the alkyne bridge is in good agreement with the calculated SOMOs and Mulliken spin density distribution (Figure 11). Interestingly, even in the case of the longest spacer (**6c**^{Menth}), the EPR parameters indicate a symmetrical delocalization of the radical along the central spacer, indicating an electron transfer process which is faster than the EPR time scale (10^{-9} s).

The mixed valence compound **6d**^{Et} was characterized by an X-ray diffraction study (Figure 12). The structure is highly symmetrical with a torsion angle of 20° between the two

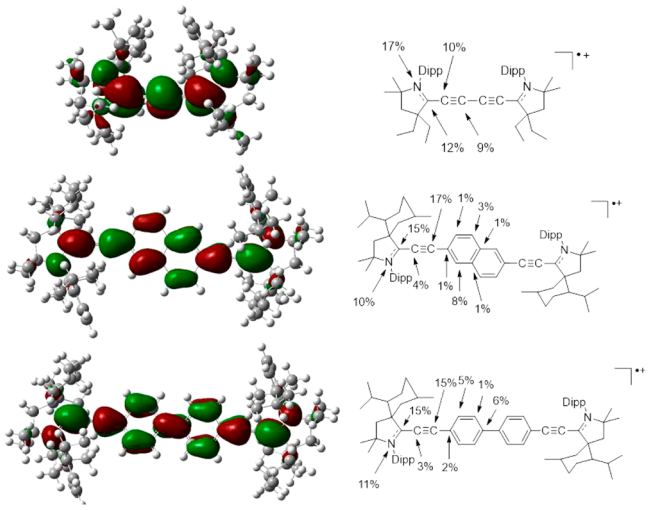

Figure 11. SOMOs of **6d**^{Et} (top) and **6b**^{Menth} (middle) (UB3LYP/def2-TZVP) and of **6c**^{Menth} (bottom) (UB3LYP/6-31G**) (isovalues 0.02) based on X-ray diffraction (**6d**^{Et}) or optimized structures (**6b**^{Menth} and **6c**^{Menth}) together with the calculated Mulliken spin densities.

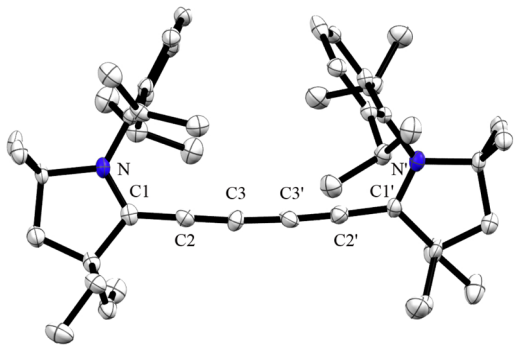

Figure 12. Solid-state structure of **6d**^{Et}. Solvent molecules, hydrogen atoms, and the counteranion (SbF_6^-) are omitted for clarity. Selected bond distances (Å) and angles (deg): N−C1 1.327(5), N′−C1′ 1.327(5), C1−C2 1.365(6), C1′−C2′ 1.368(6), C2−C3 1.235(6), C2′−C3′ 1.241(6), C3−C3′ 1.313(6), N−C1−C2 123.1(3), C1−C2−C3 177.3(4), C2−C3−C4 176.6(4), N−C1−C1′−N′ 20.0(3).

CAACs. The N−C1 bond distance [1.327(5) Å] is comparable to that observed for the radical cation **6a**^{Menth} (1.329−1.343 Å), while the C1−C2 [1.365(6) Å], C2−C3 [1.235(6)], and C3−C3′ bond lengths [1.313(6) Å] indicate a partial double bond character.

It is interesting to compare the UV−vis/NIR absorption spectra of the different MV complexes, including that of $[(^{Et}CAAC)_2C_2]^{+\bullet}$ [21] (Figure 13). The latter exhibits three main absorption bands at λ = 382/408 nm (I), 460 nm (II; broad), and 540 nm (III) and importantly no absorption in the NIR, while the higher homologue **6d**^{Et} exhibits the same band structures but with significantly red-shifted absorption bands at λ = 483 nm (I), 540 nm (II; broad), and 709 nm (III). Interestingly, the absorption at 540 nm $[(^{Et}CAAC)_2C_2]^{+\bullet}$ corresponds to the highly nonsymmetrical absorption at 709 nm (**6d**^{Et}) which flattens out into the NIR up to 1000 nm.

Even though the low-energy band only reaches into the NIR region, it seems likely, based on the cutoff shape of the absorption band (see also the Supporting Information) and the short distance between the two descrete CAAC redox centers,

DOI: 10.1021/jacs.7b11184
J. Am. Chem. Soc. 2018, 140, 2206−2213

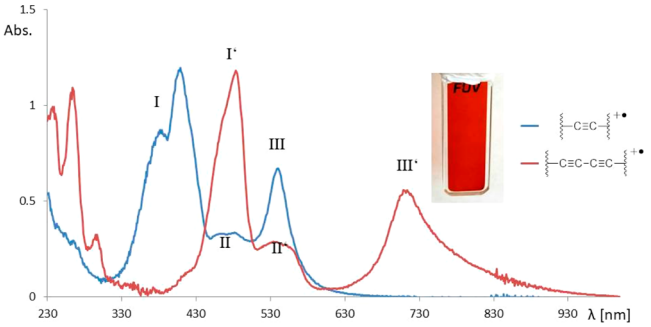

Figure 13. Comparison of the UV−vis spectra of radical cation $[(^{Et}CAAC)_2C_2]^{+\bullet}$ and $\mathbf{6d}^{Et}$ (both in CH_2Cl_2) containing −CC− and −CC−CC− spacers, respectively (inset: color of $\mathbf{6d}^{Et}$).

that $\mathbf{6d}^{Et}$ can be classified as a fully delocalized Robin−Day class III organic MV system with intermediate redox states. Alternatively, an argument based on a particle in a box might be applicable,[32] which however seems to be limited, as we observe clear redox site behavior of the CAAC moieties. Furthermore, as class III compounds can be estimated by $V = E(op)/2$, which will give large coupling integral values, another argumentation might be based on the character of bridge-localized (or biased) electrophores.[33] The absorption spectra of $\mathbf{6d}^{Et}$ show no significant solvent dependency (UV/vis-NIR spectra of $\mathbf{6d}^{Et}$ appear nearly identical in THF and CH_2Cl_2), which is also consistent with a class III system. It should be noted, while $[(^{Et}CAAC)_2C_2]^{+\bullet}$ is stable in air in CH_2Cl_2, $\mathbf{6d}^{Et}$ decomposes over ca. 2 h under identical conditions. In contrast to $\mathbf{6d}^{Et}$, $[(^{Et}CAAC)_2C_2]^{+\bullet}$ is better understood as a classical charge-resonance complex, based on the missing IV-CT band. The IR spectrum shows a significant shift of the alkyne band upon reduction from $\tilde{\nu} = 2147$ cm^{-1} (bis-iminium $\mathbf{4d}^{Et}$) to 2041 cm^{-1} ($\mathbf{6d}^{Et}$) [$(^{Et}CAAC)_2C_2)^{+\bullet}$ does not show any IR absorption in the alkyne region; see the Supporting Information]. The observation of only one IR band for $\mathbf{6d}^{Et}$ in the solid state is in agreement with an intramolecular electron transfer rate faster than 10^{-13} s, consistent with a class III mixed valence system. This is also in line with reported class III MV transition metal systems containing diyne spacers that are discussed as molecular wires for nanoscale electronic devices.[34]

When moving from the pure alkyne spacers to those containing aromatic units between the alkynes, a clear "jump" in the mixed valence IV-CT processes is detectable on the basis of UV/vis-NIR spectra (Figure 14 and Table 1).

Upon extension of the spacer, a red-field-shifted IV-CT band is detected. As observed for $\mathbf{6a}^{Et}/\mathbf{6a}^{Menth}$, compound $\mathbf{6b}^{Menth}$

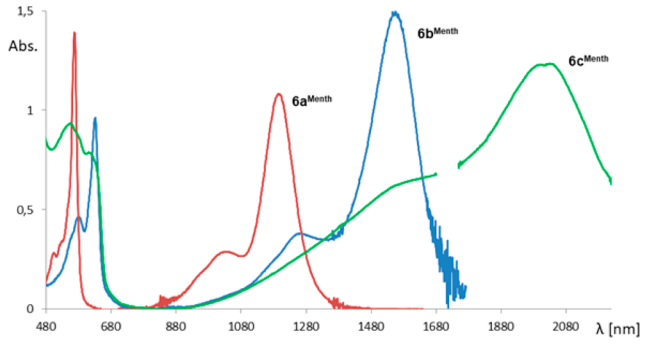

Figure 14. Comparison of the UV−vis/NIR spectra of the MV systems $\mathbf{6a-c}^{Menth}$.

Table 1. Summary of Key Parameters for Some CAAC Derived Organic Mixed Valence Compounds

	bridge	IV-CT band [cm^{-1}]	ε [cm^{-1} mol^{-1}]	"bridge-band" [cm^{-1}]	V [cm^{-1}]
$\mathbf{6a}^{Et}$	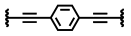	8368	43427	9804	1032
$\mathbf{6a}^{Menth}$	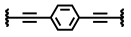	8264	41734	9588	1019
$\mathbf{6b}^{Menth}$	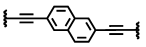	6439	61173	8000	887
$\mathbf{6c}^{Menth}$	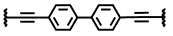	4941	17506	6180	401
$\mathbf{6d}^{Et}$		14104	---	---	---

shows an intense Gaussian shaped NIR absorption at λ_{max} = 1553 nm ($\tilde{\nu}_{max}$ = 6439 cm^{-1}) with a very similar bandwidth at half-height $\tilde{\nu}_{1/2}$ (796 cm^{-1}). On the basis of formula I, the determined molar absorptivity ε (61 173 M^{-1} cm^{-1}) and distance r (13.0 Å), the electronic coupling integral V is calculated to be 887 cm^{-1}. As expected upon extension of the spacer, the coupling integral decreases from 1019 cm^{-1} ($\mathbf{6a}^{Menth}$) to 887 cm^{-1} ($\mathbf{6b}^{Menth}$), with $2V/\lambda$ = 0.28 still indicative for a class IIa MV compound. Similar to $\mathbf{6a}^{Menth}$, the high energy NIR shoulder at λ_{max} = 1250 nm for $\mathbf{6b}^{Menth}$ can be assigned to an electron transfer process from the CAAC radical center to the spacer (three-state model). Interestingly, $\mathbf{6c}^{Menth}$ shows an intense Gaussian shaped absorption shifted far into the NIR at λ_{max} = 2024 nm ($\tilde{\nu}_{max}$ = 4941 cm^{-1}) with a broad high-energy shoulder at λ = 1618 nm ($\tilde{\nu}$ = 6180 cm^{-1}). On the basis of formula I and the parameters $\tilde{\nu}_{1/2}$ (1000 cm^{-1}),[35] ε (17 506 M^{-1} cm^{-1}), and r (15.1 Å), the coupling integral V of $\mathbf{6c}^{Menth}$ is calculated as 401 cm^{-1} (Table 1). Even though the CAAC−linker−CAAC distance is already 1.5 nm, it seems most likely based on the spectroscopic data obtained that $\mathbf{6c}^{Menth}$ can be classified as a weakly coupled class II mixed valence compound (this compound is approaching the less-well-defined region of class I/II MV compounds). It should be pointed out that the position of the IV-CT band ($\mathbf{6a-6d}$) seems to correlate exponentially with the distance between the CAAC centers (see Figure S19). It should also be highlighted that no NIR absorption is observed for any of the dications ($\mathbf{4a-c}$) or neutral compounds ($\mathbf{5a-c}$). Note that the dications usually exhibit absorptions at the UV−vis edge at 383 nm ($\mathbf{4b}^{Menth}$) and 398 nm ($\mathbf{4c}^{Menth}$) and show strong blue fluorescence in solution [emission maxima 484 nm ($\mathbf{4b}^{Menth}$), 460 nm ($\mathbf{4c}^{Menth}$)] (see the Supporting Information). We observed in the case of $\mathbf{6b}^{Menth}$ two ATR-IR absorption bands, one at $\tilde{\nu}_{CC}$ = 2180 cm^{-1} and the other, weaker, at 2065 cm^{-1}, comparable to those of the oxidized ($\mathbf{4b}^{Menth}$: 2193 cm^{-1}) and reduced ($\mathbf{5b}^{Menth}$: 2044 cm^{-1}) compounds. This observation is in agreement with a slower electron transfer process in $\mathbf{6b}^{Menth}$, compared to $\mathbf{6a}^{Menth}$, and it reaches the time scale of ATR-IR spectroscopy. Upon extension of the spacer, thereby decreasing the coupling, we observed that the sensitivity of compounds **6** toward oxygen increases. While $\mathbf{6d}^{Et}$ is stable for a few hours in air, the stability of **6a** to $\mathbf{6c}^{Menth}$ drops to seconds.

DOI: 10.1021/jacs.7b11184
J. Am. Chem. Soc. 2018, 140, 2206−2213

CONCLUSION

In summary, we have demonstrated that cyclic iminium scaffolds derived from CAACs can be used as room temperature stable carbon centered radicals for the preparation of a novel family of mixed valence compounds. The latter can be isolated and characterized by various techniques, including X-ray crystallography. Lengthening of the spacer systematically red-shifts the IV-CT band from the visible to the near-infrared. In agreement with the reduction potential separation obtained by CV, and with the coupling integrals obtained from the band shape analysis of the IV-CT bands, the spacer modulates the electron transfer from class II (**6a**–**c**) to class III (**6d**) systems. We are currently investigating applications of this novel type of MV compounds.

ASSOCIATED CONTENT

Supporting Information

The Supporting Information is available free of charge on the ACS Publications website at DOI: 10.1021/jacs.7b11184.

The experimental procedures for the synthesis of the here outlined compounds as well as their NMR, EPR, and UV–vis/NIR spectra (PDF)

CIF files for $\mathbf{6a}^{\mathbf{Menth}}$ and $\mathbf{6d}^{\mathbf{Et}}$ (ZIP)

AUTHOR INFORMATION

Corresponding Author

*guybertrand@ucsd.edu

ORCID

Mohand Melaimi: 0000-0003-3553-1381

Guy Bertrand: 0000-0003-2623-2363

Notes

The authors declare no competing financial interest.

ACKNOWLEDGMENTS

Thanks are due to the NSF (CHE-1661518) for financial support of this work and to the Alexander von Humboldt foundation for a Feodor-Lynen scholarship (M.M.H.). We are grateful to the Keck Foundation for funding the KeckII computer center, A. L. Rheingold, M. Gembicky, and C. E. Moore (X-ray diffraction), and M. Tauber (EPR). We are also in debt to T. Porter and C. Kubiak for helpful discussions.

REFERENCES

(1) (a) Winkler, J. R.; Gray, H. B. *Chem. Rev.* **1992**, *92*, 369. (b) Koval, C. A.; Howard, J. N. *Chem. Rev.* **1992**, *92*, 411.

(2) Barbara, P. F.; Meyer, T. J.; Ratner, M. A. *J. Phys. Chem.* **1996**, *100*, 13148.

(3) (a) Hush, N. S. In *Mixed-Valence Compounds*; Brown, D. B., Ed.; D. Reidel Publishing Company: Dordrecht, The Netherlands, 1980. (b) Launay, J.-P. *Chem. Soc. Rev.* **2001**, *30*, 386. (c) Richardson, D. E.; Taube, H. *Coord. Chem. Rev.* **1984**, *60*, 107.

(4) (a) Creutz, C.; Taube, H. *J. Am. Chem. Soc.* **1969**, *91*, 3988. (b) Creutz, C.; Taube, H. *J. Am. Chem. Soc.* **1973**, *95*, 1086.

(5) For excellent overviews on organic MV systems, see: (a) Hankache, J.; Wenger, O. S. *Chem. Rev.* **2011**, *111*, 5138. (b) Heckmann, A.; Lambert, C. *Angew. Chem., Int. Ed.* **2012**, *51*, 326.

(6) (a) Nelsen, S. F.; Chang, H.; Wolff, J. J.; Adamus, J. *J. Am. Chem. Soc.* **1993**, *115*, 12276. (b) Nelsen, S. F.; Tran, H. Q.; Nagy, M. A. *J. Am. Chem. Soc.* **1998**, *120*, 298. (c) Nelsen, S. F.; Ramm, M. R.; Wolf, J. J.; Powell, D. R. *J. Am. Chem. Soc.* **1997**, *119*, 6863. (d) Rak, S. F.; Miller, L. L. *J. Am. Chem. Soc.* **1992**, *114*, 1388. (e) Utamapanya, S.; Rajca, A. *J. Am. Chem. Soc.* **1991**, *113*, 9242. (f) Closs, G. L.; Miller, J. R. *Science* **1988**, *240*, 440. (g) Paddon-Row, M. N. *Acc. Chem. Res.* **1994**, *27*, 18.

(7) (a) Wurster, C. *Ber. Dtsch. Chem. Ges.* **1879**, *12*, 522. (b) Michaelis, L.; Hill, E. S. *J. Am. Chem. Soc.* **1933**, *55*, 1481. (c) Michaelis, L.; Schubert, M. P.; Granick, S. *J. Am. Chem. Soc.* **1939**, *61*, 1981.

(8) (a) Coffen, D. L.; Chambers, J. Q.; Williams, D. R.; Garrett, P. E.; Canfield, N. D. *J. Am. Chem. Soc.* **1971**, *93*, 2258. (b) Wudl, F.; Wobschal, D.; Hufnagel, E. J. *J. Am. Chem. Soc.* **1972**, *94*, 670. (c) Lahlil, K.; Moradpour, A.; Bowlas, C.; Menou, F.; Cassoux, P.; Bonvoisin, J.; Launay, J. P.; Dive, G.; Dehareng, D. *J. Am. Chem. Soc.* **1995**, *117*, 9995.

(9) Hünig, S. *Pure Appl. Chem.* **1967**, *15*, 109.

(10) Robin, M. B.; Day, P. *Adv. Inorg. Chem. Radiochem.* **1968**, *10*, 247.

(11) Hush, N. S. *Coord. Chem. Rev.* **1985**, *64*, 135.

(12) (a) Brunschwig, B. S.; Creutz, C.; Sutin, N. *Chem. Soc. Rev.* **2002**, *31*, 168. (b) Brunschwig, B. S.; Sutin, N. *Coord. Chem. Rev.* **1999**, *187*, 233.

(13) See, for example: (a) Lambert, C.; Nöll, G. *J. Am. Chem. Soc.* **1999**, *121*, 8434. (b) Schäfer, J.; Holzapfel, M.; Mladenova, B.; Kattnig, D.; Krummenacher, I.; Braunschweig, H.; Grampp, G.; Lambert, C. *J. Am. Chem. Soc.* **2017**, *139*, 6200. (c) Lambert, C.; Nöll, G. *Angew. Chem., Int. Ed.* **1998**, *37*, 2107. (d) Bonvoisin, J.; Launay, J. P.; Van der Auweraer, M.; De Schryver, F. C. *J. Phys. Chem.* **1994**, *98*, 5052.

(14) (a) Bonvoisin, J.; Launay, J.-P.; Rovira, C.; Veciana, J. *Angew. Chem., Int. Ed. Engl.* **1994**, *33*, 2106. (b) Rovira, C.; Ruiz-Molina, D.; Elsner, O.; Vidal-Gancedo, J.; Bonvoisin, J.; Launay, J.-P.; Veciana, J. *Chem. - Eur. J.* **2001**, *7*, 240.

(15) Rosokha, S. V.; Sun, D. L.; Kochi, J. K. *J. Phys. Chem. A* **2002**, *106*, 2283.

(16) For the synthesis of CAACs, see: (a) Lavallo, V.; Canac, Y.; Präsang, C.; Donnadieu, B.; Bertrand, G. *Angew. Chem., Int. Ed.* **2005**, *44*, 5705. (b) Jazzar, R.; Dewhurst, R. D.; Bourg, J. B.; Donnadieu, B.; Canac, Y.; Bertrand, G. *Angew. Chem., Int. Ed.* **2007**, *46*, 2899. (c) Tomás-Mendivil, E.; Hansmann, M. M.; Weinstein, C. M.; Jazzar, R.; Melaimi, M.; Bertrand, G. *J. Am. Chem. Soc.* **2017**, *139*, 7753.

(17) For reviews, see: (a) Melaimi, M.; Jazzar, R.; Soleilhavoup, M.; Bertrand, G. *Angew. Chem., Int. Ed.* **2017**, *56*, 10046. (b) Soleilhavoup, M.; Bertrand, G. *Acc. Chem. Res.* **2015**, *48*, 256. (c) Paul, U. S. D.; Radius, U. *Eur. J. Inorg. Chem.* **2017**, *2017*, 3362. (d) Melaimi, M.; Soleilhavoup, M.; Bertrand, G. *Angew. Chem., Int. Ed.* **2010**, *49*, 8810. (e) Droege, T.; Glorius, F. *Angew. Chem., Int. Ed.* **2010**, *49*, 6940. (f) Hahn, F. E.; Jahnke, M. C. *Angew. Chem., Int. Ed.* **2008**, *47*, 3122. (h) Roy, S.; Mondal, K. C.; Roesky, H. W. *Acc. Chem. Res.* **2016**, *49*, 357.

(18) (a) Mahoney, J. K.; Martin, D.; Moore, C. E.; Rheingold, A. L.; Bertrand, G. *J. Am. Chem. Soc.* **2013**, *135*, 18766. (b) Mahoney, J. K.; Martin, D.; Thomas, F.; Moore, C. E.; Rheingold, A. L.; Bertrand, G. *J. Am. Chem. Soc.* **2015**, *137*, 7519. (c) Mahoney, J. K.; Jazzar, R.; Royal, G.; Martin, D.; Bertrand, G. *Chem. - Eur. J.* **2017**, *23*, 6206.

(19) See, for example: (a) Weinberger, D. S.; Melaimi, M.; Moore, C. E.; Rheingold, A. L.; Frenking, G.; Jerabek, P.; Bertrand, G. *Angew. Chem., Int. Ed.* **2013**, *52*, 8964. (b) Singh, A. P.; Samuel, P. P.; Roesky, H. W.; Schwarzer, M. C.; Frenking, G.; Sidhu, N. S.; Dittrich, B. *J. Am. Chem. Soc.* **2013**, *135*, 7324. (c) Mondal, K. C.; Samuel, P. P.; Roesky, H. W.; Carl, E.; Herbst-Irmer, R.; Stalke, D.; Schwederski, B.; Kaim, W.; Ungur, L.; Chibotaru, L. F.; Hermann, M.; Frenking, G. *J. Am. Chem. Soc.* **2014**, *136*, 1770. (d) Ung, G.; Rittle, J.; Soleilhavoup, M.; Bertrand, G.; Peters, J. C. *Angew. Chem., Int. Ed.* **2014**, *53*, 8427. (e) Mondal, K. C.; Roesky, H. W.; Schwarzer, M. C.; Frenking, G.; Tkach, I.; Wolf, H.; Kratzer, D.; Herbst-Irmer, R.; Niepötter, B.; Stalke, D. *Angew. Chem., Int. Ed.* **2013**, *52*, 1801. (f) Abraham, M. Y.; Wang, Y.; Xie, Y.; Gilliard, R. J., Jr.; Wei, P.; Vaccaro, B. J.; Johnson, M. K.; Schaefer, H. F., III; Schleyer, P. v. R.; Robinson, G. H. *J. Am. Chem. Soc.* **2013**, *135*, 2486. (g) Kretschmer, R.; Ruiz, D. A.; Moore, C. E.; Rheingold, A. L.; Bertrand, G. *Angew. Chem., Int. Ed.* **2014**, *53*, 8176. (h) Martin, D.; Moore, C. E.; Rheingold, A. L.; Bertrand, G. *Angew.*

DOI: 10.1021/jacs.7b11184
J. Am. Chem. Soc. 2018, 140, 2206–2213

Chem., Int. Ed. **2013**, *52*, 7014. (i) Roy, S.; Stückl, A. C.; Demeshko, S.; Dittrich, B.; Meyer, J.; Maity, B.; Koley, D.; Schwederski, B.; Kaim, W.; Roesky, H. W. *J. Am. Chem. Soc.* **2015**, *137*, 4670.
(20) For reviews, see: (a) Martin, C. D.; Soleilhavoup, M.; Bertrand, G. *Chem. Sci.* **2013**, *4*, 3020. (b) Mondal, K. C.; Roy, S.; Roesky, H. W. *Chem. Soc. Rev.* **2016**, *45*, 1080.
(21) (a) Li, Y.; Mondal, K. C.; Samuel, P. P.; Zhu, H.; Orben, C. M.; Panneerselvam, S.; Dittrich, B.; Schwederski, B.; Kaim, W.; Mondal, T.; Koley, D.; Roesky, H. W. *Angew. Chem., Int. Ed.* **2014**, *53*, 4168. (b) Jin, L.; Melaimi, M.; Liu, L.; Bertrand, G. *Org. Chem. Front.* **2014**, *1*, 351.
(22) Munz, D.; Chu, J.; Melaimi, J.; Bertrand, G. *Angew. Chem., Int. Ed.* **2016**, *55*, 12886.
(23) Hansmann, M. M.; Melaimi, M.; Munz, D.; Bertrand, G. *J. Am. Chem. Soc.* **2018**, DOI: 10.1021/jacs.7b11183.
(24) Hansmann, M. M.; Melaimi, M.; Bertrand, G. *J. Am. Chem. Soc.* **2017**, *139*, 15620.
(25) The winsim 2012 software was used: Duling, D. R. *J. Magn. Reson., Ser. B* **1994**, *104*, 105.
(26) Renz, M.; Theilacker, K.; Lambert, C.; Kaupp, M. *J. Am. Chem. Soc.* **2009**, *131*, 16292.
(27) Note that the geometrical distance between the CAAC moieties might not be accurate to derive the coupling integral, as Nelsen et al. pointed out that the number of bonds between the redox centers is more representative: Nelsen, S. F.; Tran, H. Q.; Nagy, M. A. *J. Am. Chem. Soc.* **1998**, *120*, 298. Therefore, the effective distance can be significantly shorter than the geometrical distance, leading to a larger coupling integral V.
(28) See also: Lambert, C.; Nöll, G. *J. Am. Chem. Soc.* **1999**, *121*, 8434.
(29) (a) Cotton, F. A.; Hush, N. S. *Prog. Inorg. Chem.* **1967**, *8*, 391. (b) Kubiak, C. P. *Inorg. Chem.* **2013**, *52*, 5663. (c) Ito, T.; Hamaguchi, T.; Nagino, H.; Yamaguchi, T.; Washington, J.; Kubiak, C. P. *Science* **1997**, *277*, 660.
(30) (a) Le Narvor, N.; Lapinte, C. *Organometallics* **1995**, *14*, 634. (b) Stang, P. J.; Tykwinski, R. *J. Am. Chem. Soc.* **1992**, *114*, 4411.
(31) (a) D'Alessandro, D. M.; Keene, F. R. *Chem. Soc. Rev.* **2006**, *35*, 424. (b) Linseis, M.; Zalis, S.; Zabel, M.; Winter, R. F. *J. Am. Chem. Soc.* **2012**, *134*, 16671. (c) Zhong, Y.-W.; Gong, Z.-L.; Shao, J.-Y.; Yao, J. *Coord. Chem. Rev.* **2016**, *312*, 22.
(32) Shalhoub, G. M. *J. Chem. Educ.* **1997**, *74*, 1317.
(33) See, for example: Tang, J.-H.; Shao, J.-Y.; He, Y.-Q.; Wu, S.-H.; Yao, J.; Zhong, Y.-W. *Chem. - Eur. J.* **2016**, *22*, 10341.
(34) (a) Bruce, M. I.; Low, P. J.; Costuas, K.; Halet, J.-F.; Best, S. P.; Heath, G. A. *J. Am. Chem. Soc.* **2000**, *122*, 1949. (b) Brady, M.; Weng, W.; Zhou, Y.; Seyler, J. W.; Amoroso, A. J.; Arif, A. M.; Böhme, M.; Frenking, G.; Gladysz, J. A. *J. Am. Chem. Soc.* **1997**, *119*, 775. (c) Halet, J. F.; Lapinte, C. *Coord. Chem. Rev.* **2013**, *257*, 1584.
(35) $\tilde{\nu}_{1/2}$ was determined from doubling the energy difference between $\tilde{\nu}_{max}$ and the half-height at the low energy site.

DOI: 10.1021/jacs.7b11184
J. Am. Chem. Soc. 2018, 140, 2206−2213